

Relaxation, Recovery, Crystallization, and Recrystallization Transformations in an Iron Based Amorphous Precursor

B.B. Kappes^a, B.E. Meacham^{a*}, Y.L. Tang^b, D.J. Branagan^{a*}

^a*Idaho National Engineering and Environmental Laboratories, Idaho Falls, ID 83415-2218 USA*
^b*Argonne National Laboratory, Argonne, IL 60439, USA*

Abstract

The focus of this research was on gaining a fundamental understanding of the structure/property relationships that exist in an iron based multicomponent glass forming alloy. While composition is one key parameter in determining the final microstructure, the specific transformation conditions (temperature and time) how a glass devitrifies was found to have significant effects on the development of the devitrified microstructure. Microstructural studies have revealed that recovery, relaxation, crystallization, and recrystallization phenomena are important effects which lead to large differences in the resulting microstructure resulting in significant differences in properties such as devitrified hardness. The information gained in this study, combined with further investigation into the mechanistic processes governing these transformations, may allow for the further development of nanostructured materials with targeted sets of properties.

1. Introduction

Relaxation in metallic glasses has been studied for the last thirty years.^{1,2,3,4,5} The atomic rearrangement characteristic of structural relaxation has been shown to have a significant effect on many properties of the metallic glass, including density⁶, Curie temperature⁷, and deformation response⁸, among others.⁹ Several theories and models have been developed to explain the behavior of metallic systems during the relaxation process.^{10,11,12,13} From these, morphological and phenomenological aspects of metallic glasses have been identified as significant in the relaxation process, including formation of free volume during rapid solidification, the annihilation of free volume upon annealing, and the temperature dependent thermodynamic stability of the glass.

The existence of free volume in the glass has several consequences in regards to structural relaxation. The trapped free volume is analogous to vacancies in a crystal lattice with similar effects on the local properties of the material. As mentioned earlier, Frank et al.¹⁴ examined the effect of relaxation on the substitutional diffusion characteristics of several metallic glasses. Regions of free volume act to increase the diffusivity of transition metals at a given temperature by an exchange mechanism wherein either a single atom or cluster of atoms jump to occupy the void, effectively transporting the free volume through the sample.

Due to the property dependence on the free volume concentration, the annihilation of free volume at the sample surface upon annealing causes significant changes in the diffusion characteristics of the material. As the quantity of free volume decreases, the diffusivity of the transition metal species also decreases. However, the time-dependent nature of substitutional

* Currently employed with The NanoSteel Company

diffusion does not carry over to interstitial diffusion since the mobility of interstitials, such as C and B, is dependent on the average size of the interstitial sites, which does not change dramatically during relaxation.^{15,16,17}

The activation energy spectrum (AES) model^{18,19} attributes specific activation energies to particular transitions, which, when combined with all possible transitions available in the amorphous sample, form an activation energy spectrum, analogous to electronic band theory. As a result, the number and type of transitions available to a sample is dependant on the sample annealing temperature. The thermodynamic stability of the glass is a measure of the ability of the glass to resist transformation during annealing, which can then be further classified into the stability of the glass to resist crystallization, the glass transition, or the wealth of phenomena responsible for relaxation.

This study sought to examine and explain the effects of relaxation and recovery on the morphological properties of an iron-based amorphous alloy after low-temperature annealing alone and following a subsequent crystallization step. The resulting structure was then compared to the changes in the physical properties of the material to provide insight into the structure/property relationships fundamental to materials development and ultimately for technological utilization of nanostructured materials derived from an amorphous precursor.

2. Experimental Procedure

The alloy composition chosen for this study had the atomic stoichiometry of $(\text{Fe}_{0.8}\text{Cr}_{0.2})_{79}\text{B}_{17}\text{W}_2\text{C}_2$. The targeted alloy was processed from high purity constituents (>99.9%) into ribbons by melt-spinning in 1/3 atm ultra high purity (UHP) He at a tangential wheel velocity of 15 m/s. Heat-treating was done on ribbon samples in a vacuum tube furnace at 10^{-6} torr. A summary of the samples and their respective heat treatment parameters is given in Table 1. Differential thermal analysis of the ribbon samples was performed in a Perkin Elmer DTA-7 from 30°C to 1375°C at a heating rate of 10°C/min in a 20 ml/s flow-rate of UHP Ar. X-ray diffraction (XRD) was carried out on powdered samples after incorporation of a silicon standard using a Bruker X-ray Diffractometer with Cr-K_α radiation. Analysis of the experimental X-ray patterns was done by Rietveld analysis using SIROQUANT V 2.0 software and the calculated patterns were refined until the total χ^2 was less than 3.5 over the entire two-theta range (40°-150°). Transmission Electron microscopy (TEM) was performed on a Philips CM30T analytical electron microscope with an attached EDAX energy dispersive spectrometer (EDS) using an ultra thin window detector. TEM samples were first polished from the free side of the ribbons to reduce the thickness to approximately 20 μm , dimpled and then ion milled by a Gatan PIPS low angle ion mill from two directions. For composition analysis using EDS, a separate spectrum was collected for the beam directed through the hole of each thin specimen and then this ‘hole count’ was subtracted from the unknown and standard spectra to minimize effects of spurious X-ray generation within the microscope. Peak intensities were converted to compositions using the Cliff–Lorimer approach,

$$\frac{I_A}{I_B} = k_{AB} \frac{C_A}{C_B} \quad \text{Equation 1}$$

where B is the base element (iron in this case) for which the k-factors are determined.²⁰ Convergent beam electron diffraction was employed to analyze the structure and identify the

nano-sized phases. The magnetic properties of the sample were determined using a Lakeshore vibrating sample magnetometer (VSM). The sample was ramped to 23 kOe in 5 kOe increments to determine the saturation magnetization. The field was then reduced to 1000 Oe and ramped to -1000 Oe with a step size of 20 Oe to provide data on the dynamic demagnetization behavior.

3. Results

Properties of the As-Spun sample

X-ray diffraction of the as-spun ribbon shows a diffuse peak centered at roughly $70^\circ 2\theta$, indicative of the broad nearest neighbor spacing distribution characteristic of a metallic glass (Figure 1(d)). The lack of defined peaks, the peaks from the silicon standard notwithstanding, indicates an absence of crystalline material detectable using this method.

Due to the indication of an amorphous phase from the XRD results, the information available through examination of the thermal properties of devitrification was of interest. Differential thermal analysis of the as-spun ribbon, seen in Figure 2, reveals a crystallization enthalpy of -141 J/g, indicative of a highly metastable glass.

Thermal Processing and Analysis

Thermal processing of the alloy can be further subdivided into 1- and 2-step anneals. Intuitively, the 1-step anneals are those samples that undergo a single thermal processing step, either low-temperature (below the crystallization onset temperature) or high-temperature annealing (above the crystallization onset temperature). The 2-step anneals processed in this study undergo a low-temperature anneal followed by a high-temperature anneal.

1-Step Anneals

Analysis of XRD scans taken after 1-step anneals at 300° , 400° , and 500°C for 100 hours reveals the development of two phases, Fe_3B and $\alpha\text{-Fe}$ (Figure 1). It is clear from these scans that the volume fraction crystallized varies proportionally to the low-temperature annealing temperature, reaching a high crystalline fraction during the 500°C 1-step anneal. Further investigation using TEM and SADP (selected area diffraction patterns) reveals that the 300° and 400°C 1-step anneal samples display the featureless morphology and diffuse ring pattern characteristic of an amorphous material (Figure 3).

Transmission electron microscopy and SADP were used to further study the microstructure of the 500°C 1-step anneal sample. This sample, seen in Figure 4, shows the development of a very unusual microstructure characterized by different microstructural scales. Selected area diffraction patterns identify that the large (≈ 2 to $5\ \mu\text{m}$) grains seen at 42 kX magnification are Fe_3B . At increased magnification, these large grains are composed of aligned Fe_3B subgrains whose size is in the range of 20 to 50 nm with roughly equidimensional $\alpha\text{-Fe}$ particles dispersed throughout the sample. The spotted ring patterns seen in the SADP are attributed to the randomly aligned $\alpha\text{-Fe}$ phase, but their diffuse character may also indicate the presence of a small volume fraction amorphous phase.

The as-spun 1-step anneal sample (see Table 1) was examined in TEM and XRD to observe the microstructural development of the as-spun specimen following a high-temperature heat

treatment. The TEM results show the formation of an isotropic, homogeneous microstructure consisting of three primary phases whose average grain size is approximately 100 to 200 nm (Figure 5). These three phases were subsequently identified as Fe_3B , Fe_{23}C_6 , and $\alpha\text{-Fe}$ using Rietveld analysis of the XRD scan for the as-spun 1-step anneal sample. Previous work²¹ has shown that the phases in this alloy are also easily identified by their unique morphologies. The Fe_{23}C_6 is featureless, the $\alpha\text{-Fe}$ appears mottled, and the Fe_3B forms a heavily twinned structure during high-temperature annealing. These observations provide a foundation for comparison to the structure identified in the 2-step anneals, discussed presently.

2-Step Anneals

The samples heat-treated at 300°, 400°, and 500°C were examined again in the TEM after annealing at 700°C for 10 minutes (Figure 6). The microstructure observed in the 2-step anneals form the Fe_3B , $\alpha\text{-Fe}$, and Fe_{23}C_6 phases similar to those observed in the as-spun 1-step anneal sample; however, the 2-step anneal samples also include 20 to 50 nm $\alpha\text{-Fe}$ nanoparticles similar to those seen in the 300°, 400°, and 500°C 1-step anneals (Figure 7). Of particular note is the distribution of these nanoparticles since they are not relegated to interfacial boundaries, but are also found within the Fe_3B , Fe_{23}C_6 , and large $\alpha\text{-Fe}$ grains. In comparison to the as-spun 1-step anneal sample, microhardness measurements show an unequivocal increase in hardness after the 2-step annealing process (Figure 8). This augmented hardness abates slowly with increased low-temperature annealing temperature and with the subsequent increase in the average size of the $\alpha\text{-Fe}$ nanoparticles (Figure 7).

4. Discussion

As discussed in the *Introduction*, relaxation in metallic glasses is an extensively studied, yet poorly understood phenomenon. The properties of the glass can be significantly affected as a result of structural relaxation, which reduces the free energy of the amorphous material to create a more thermodynamically stable structure.²² The high metastability of the $(\text{Fe}_{0.8}\text{Cr}_{0.2})_{79}\text{B}_{17}\text{W}_2\text{C}_2$ amorphous alloy provides a large driving force for both relaxation and crystallization below the measured crystallization onset temperature of 536°C.

Structural Transformation Phenomena

Relaxation Phenomena

Magnetic properties are exceptionally sensitive to both compositional and morphological features, which infer that structural relaxation may have a noticeable effect on the magnetic properties of the samples. Table 2 verifies this expectation by revealing an order-of-magnitude variability in the saturation magnetization and coercivity of selected samples as a function of thermal processing parameters. The ferromagnetic properties of the as-spun material after annealing at 300°C are reduced significantly and exhibit primarily a paramagnetic response. This ferromagnetic-to-paramagnetic transition is believed to be due to the equilibration of the C and B concentrations and the short-range redistribution of the transition metal elements during structural relaxation at 300°C. The resulting changes in both the local chemical and topological short-range order significantly affects the magnetic properties (for example, by lowering the Curie temperature below room temperature) with only a minimal change in the structure of material as measured with XRD, TEM, and SADP techniques. The magnetic properties then increase contemporaneously with increased low-temperature annealing.

Crystallization Phenomena

It is traditionally thought that devitrification begins at the crystallization onset temperature. However, examination of the XRD, TEM, and SADP data indicates that crystallization can occur at temperatures significantly below the onset temperature. Under the thermal processing conditions described previously, the thermodynamically stable Fe₃B system was found to form preferentially during low-temperature annealing. It is thought that this phase forms first since it is closest to the stoichiometry of the starting alloy and can form while minimizing the degree of Fe diffusion necessary to crystallize the glass precursor. Additionally, the α -Fe nanoparticles formed as a result of the hyperstoichiometric concentration of Fe in the amorphous phase with respect to the Fe₃B alloy. The growth of the α -Fe nanoparticles is subsequently restricted by the limited mobility of Fe at these low-temperature anneals. This is further supported by VSM studies conducted on a select set of samples (Figure 9). From the deterioration and subsequent development of the magnetic properties of the investigated alloy, the link between the microstructure of a material and its magnetic behavior, established recently in work by Meacham, *et al.*²³ shows a connection between the increasing crystalline fraction present in the alloy and the progressive strengthening of the ferromagnetic properties. With the exception of the 300°C 1-step anneal sample, which exhibits insufficient ferromagnetic properties for comparison, analysis of the 1-step anneal susceptibility curves (Figure 9) indicates the formation of a ferromagnetic phase that reverses in the first quadrant. Note that in the as-spun 1-step anneal this peak in the first quadrant is not present. However, after two-step annealing, the peak in the first quadrant is present in all of the heat treated samples similar to what is shown in the 300°C 2-step anneal sample. Consequently, the ferromagnetic phase reversing in the first quadrant is identified as the α -Fe nanoparticles crystallized during low-temperature annealing and which remain in the two-step anneals. The broad peaks between -500 and -700 Oe result from the reversal of the remaining ferromagnetic phases.

The formation of these structures is aided by diffusion behavior in the system. Upon annealing at 300°C for 100 hours, the initial diffusivity of the transition metals would be higher than the diffusivity in the relaxed amorphous state, D_R .²⁴ The drop in diffusivity is due to the annihilation of free volume during annealing. This would permit sufficient transport of the transition metal elements early in the transformation to allow for the limited crystallization observed in the 300°C 1-step anneal. As the instantaneous diffusivity approaches D_R , the restricted diffusion would preclude extensive changes in the long range ordering of the transition metal elements; however, the extended time and available thermal energy would be sufficient for the long range equilibration of the concentration of the light elements, B and C. The 400°C 1-step anneal sample would lead to a similar redistribution of the light elements but would provide the thermal energy necessary to utilize the higher energy diffusion pathways. This would account for the higher degree of Fe₃B and α -Fe crystallization seen in the 400°C 1-step anneal sample. The 500°C 1-step anneal activates additional, higher energy pathways allowing for more extensive crystallization (Figure 4).

Examination of the microstructure of the 500°C 1-step anneal clarifies the mechanisms responsible for crystallization at the low-temperature anneals. Redistribution of C and B leads to the creation of locally stoichiometric Fe₃B regions throughout the material that allows for nucleation and growth of the Fe₃B phase without significant diffusion of the transition metal

elements. The size of these Fe₃B subgrains is limited to the 20 to 50 nm range; however, SADP taken during TEM examination reveals that these are almost perfectly aligned subgrains of larger 2 to 5 μm Fe₃B grains. Consequently, the orientation of subgrains nucleated later in the transformation process must be influenced by those that nucleated earlier (e.g. via heterogeneous nucleation), by the structure of the amorphous matrix, or both.

Alternatively, the high stresses inherent in metallic glasses²⁵ could create the conditions necessary for a shear induced massive transformation. This transformation could account for the military rearrangement of atoms necessary to form grains on a 2 to 5 μm scale while creating slightly misoriented subgrains based on the limited diffusion characteristics of martensitic transformations.

While each hypothesis explains the microstructure observed in the low-temperature anneals, there are several details that remain unclear and would require further investigation to determine which, if either, is correct; for example, investigation of the growth dynamics via examination of the crystal structure as a function of time at constant low-temperature annealing.

Recrystallization Phenomena

The structure and morphology of the 2-step anneal samples have been described previously; however, of particular note is the formation of the isotropic, nanometer scale grain structure during high-temperature annealing from the aligned nanoscale subgrains formed during the low-temperature annealing at 500°C. During high-temperature annealing, the transformation from a textured structure to an isotropic structure indicates that a process analogous to the recovery and recrystallization observed during annealing of cold-worked, crystalline metals²⁶ occurs to create the final, isotropic grain structure seen in the 2-step alloys. Further research is necessary to clarify the mechanism and driving force for this transformation.

The high-temperature anneal samples studied show a number of common microstructural features. First, the phase composition, within the scope of this study, remains consistent. All four samples (the as-spun 1-step anneal sample and the 300°, 400°, and 500°C 2-step anneal samples) form α-Fe, Fe₃B, and Fe₂₃C₆ phases. Of these phases, the α-Fe and Fe₃B are also seen in the low-temperature anneal samples. As mentioned earlier, the Fe₃B phase is easily identified in the samples that have undergone high-temperature annealing by the formation of a heavily twinned structure; however, the 20 to 50 nm Fe₃B seen in the 500°C 1-step anneal sample does not display this same twinning phenomenon. This suggests that the twinning in the Fe₃B is likely caused by solid-state stress created during the effective simultaneous crystallization of the Fe₂₃C₆, α-Fe, and Fe₃B phases formed during high-temperature annealing. Twinning in the Fe₃B serves as a mechanism to minimize these stresses as well as the interfacial strain created during the formation of the multiphase matrix structure. This would indicate that the increased thermal energy available at 700°C allows for the diffusion, deformation, and other transformational phenomena responsible for the formation of the complex Fe₂₃C₆ crystal structure.

Structure/Property Relationships

Regardless of the details of the transformation mechanism, relaxation, recovery, crystallization, and recrystallization processes clearly have an effect on the final properties of the alloy. The hardness in the as-spun sample annealed at 700°C is attributed to many factors including the fine

(100-200 nm) microstructure, the level of supersaturation, and the internal stress created during solid-state transformations. Since the 300°, 400°, and 500°C 2-step anneal samples possess, roughly, the same microstructural features as the as-spun 1-step anneal sample, the increased hardness seen in the 2-step anneals is apparently due to the formation of the α -Fe nanoparticles described previously. While the results of the mechanism itself is yet unclear, the α -Fe nanoparticles appear to behave as Zener pinning sites that can serve to limit grain growth during elevated temperature elongation studies, resulting in the ability to achieve low temperature superplasticity.²⁷

5. Conclusions

It has been shown that low temperature relaxation prior to high temperature annealing can have a profound, positive effect on the hardness of the investigated alloy by modifying the chemical and topological structure of the as-spun sample. This modification has also been shown to exhibit a temperature dependence in both the morphology of the low-temperature anneal samples and in the properties of the material following high-temperature annealing. The 1-step anneal samples show evidence of relaxation and, in the case of the 500°C 1-step anneal, nearly complete crystallization below the crystallization onset temperature. The 2-step anneals add recovery and recrystallization to the list of transformation phenomena by converting an aligned Fe₃B microstructure into a multiphase isotropic microstructure. The information gained in this study combined with further investigation into the mechanistic processes governing these transformations may allow for the development of nanostructured materials with targeted sets of properties for specific industrial uses.

6. Acknowledgements

Research was supported through the Defense Advanced Research Projects Agency (DARPA) under the DOE Idaho Operations Office Contract No. DE-AC07-99ID13727. TEM studies were done at the Electron Microscopy Center at Argonne National Laboratory and the authors thank Dean Miller, director of the TEM center for his support in the use of these facilities. Argonne is operated by the University of Chicago under Contract No. W-31-109-ENG-38. This document has been approved for public release, distribution unlimited.

Table 1 Summary of Heat-Treatments and Corresponding Nomenclature

Sample Identification	First Step		Second Step	
	<i>Temp (°C)</i>	<i>Time</i>	<i>Temp (°C)</i>	<i>Time</i>
As-spun ribbon	--	--	--	--
<i>1-Step Anneal Samples</i>				
As-spun 1-step anneal	700	10 min	--	--
300°C 1-step anneal	300	100 hrs	--	--
400°C 1-step anneal	400	100 hrs	--	--
500°C 1-step anneal	500	100 hrs	--	--
<i>2-Step Anneal Samples</i>				
300°C 2-step anneal	300	100 hrs	700	10 min
400°C 2-step anneal	400	100 hrs	700	10 min
500°C 2-step anneal	500	100 hrs	700	10 min

Table 2 Summary of Magnetic Properties

Sample Identification	Saturation Magnetization [G]	Coercivity [Oe]
As-spun sample	4,720	-330
300°C 1-step anneal sample	430	-60
400°C 1-step anneal sample	1,980	-410
500°C 1-step anneal sample	5,200	-460
As-spun 1-step anneal sample	5,180	-500
300°C 2-step anneal sample	5,110	-430

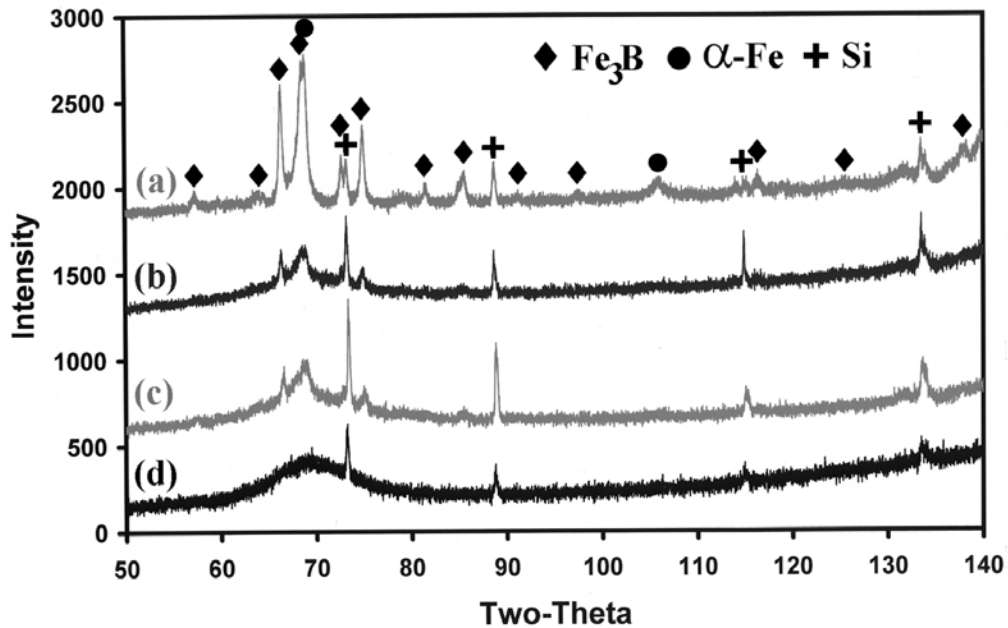


Figure 1 X-ray diffraction patterns of the $(\text{Fe}_{0.8}\text{Co}_{0.2})_{79}\text{B}_{17}\text{W}_2\text{C}_2$ alloy after (a) 500°C, (b) 400°C, and (c) 300°C anneals for 100 hours showing the development of the fraction transformed as a function of annealing temperature in comparison to the (d) as-spun material.

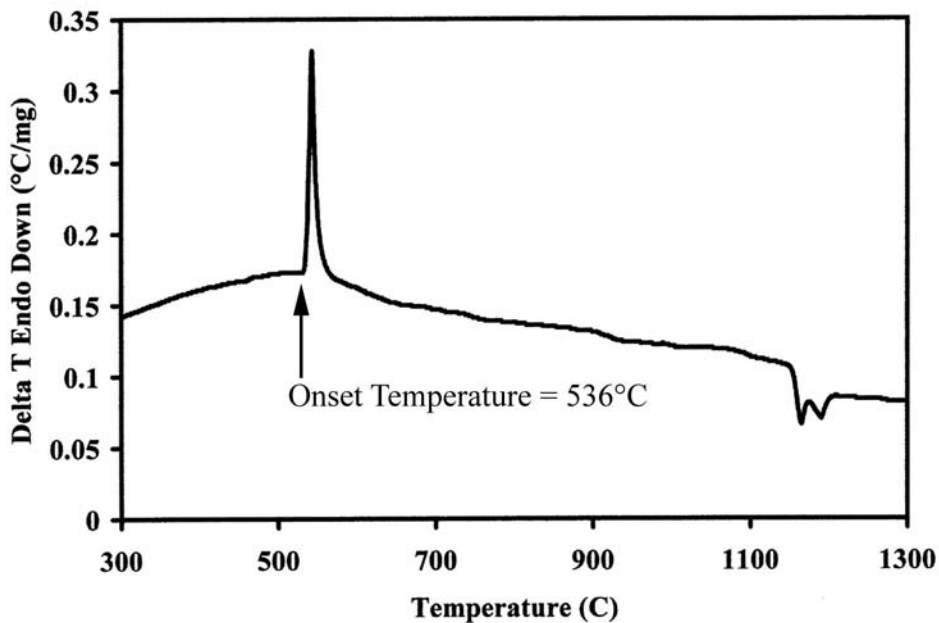


Figure 2 Differential thermal analysis of the as-spun $(\text{Fe}_{0.8}\text{Co}_{0.2})_{79}\text{B}_{17}\text{W}_2\text{C}_2$ alloy showing a single crystallization event at an onset temperature of 536°C.

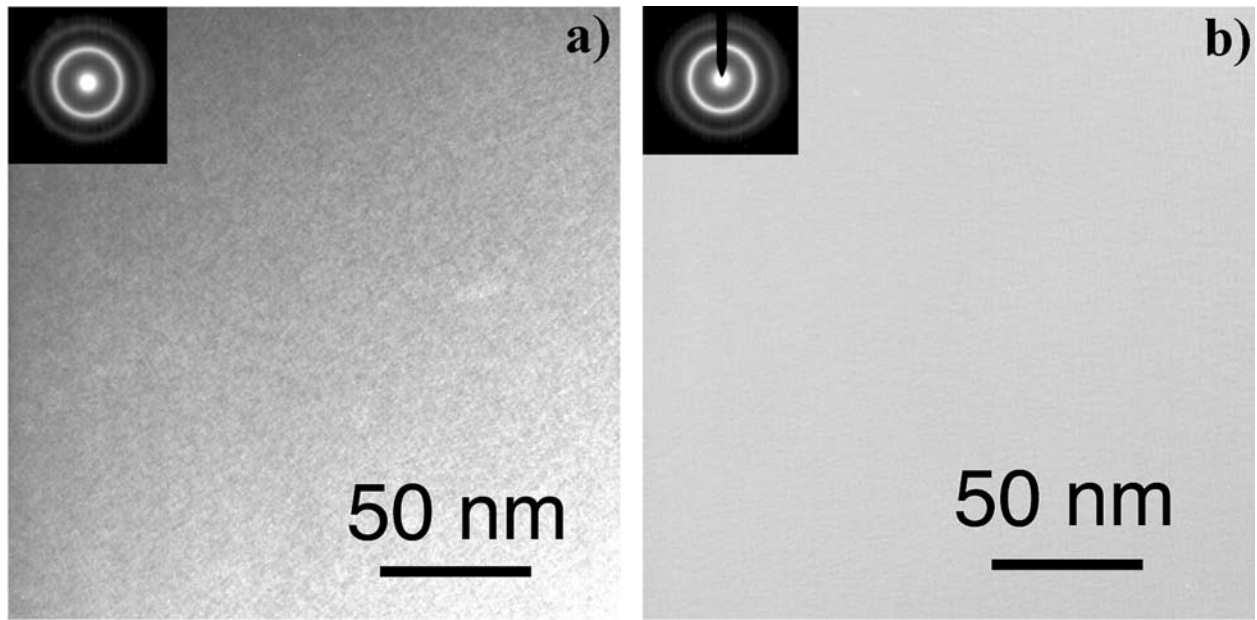


Figure 3 Transmission electron micrographs and SADP (inset) of the (a) 300° and (b) 400°C 1-step anneal samples exhibiting the featureless morphology and diffuse ring pattern characteristic of an amorphous material.

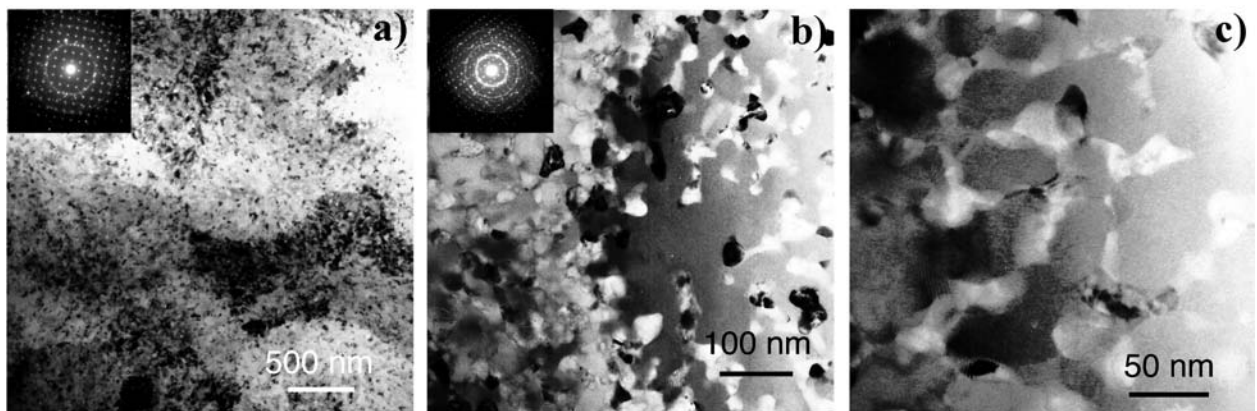


Figure 4 Transmission electron micrographs and select SADP (inset) of the 500°C 1-step anneal sample at (a) 42 kX, (b) 89 kX, and (c) 120kX magnification showing the untwinned Fe_3B phase (2-5 μm grains and 20-50 nm subgrains), 20-50 nm $\alpha\text{-Fe}$ nanoparticles, and residual amorphous phase.

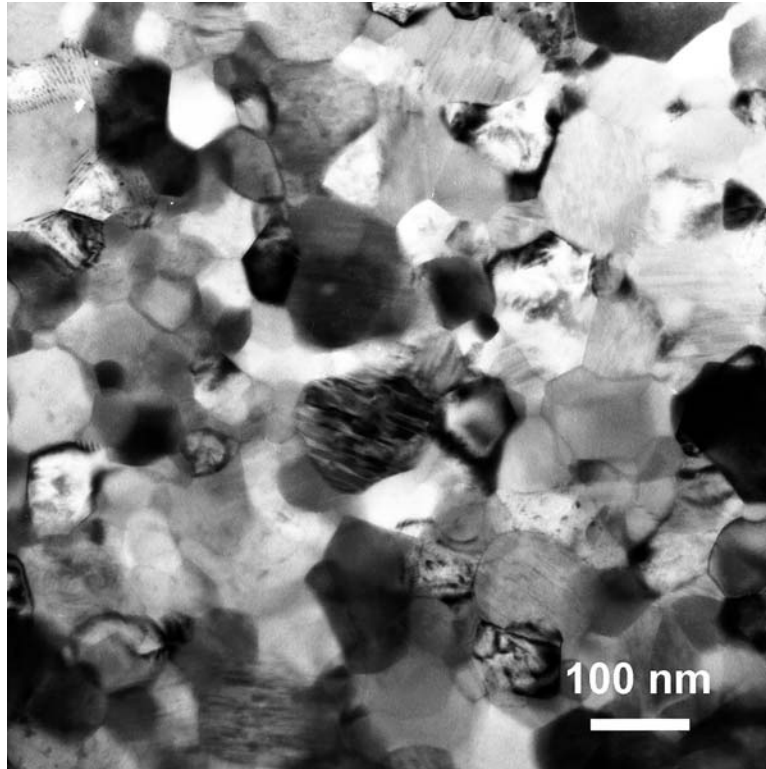


Figure 5 Transmission electron microscopy of the as-spun 1-step anneal sample showing the isotropic formation of 100 to 200 nm Fe_3B (heavily twinned), Fe_{23}C_6 (featureless), and $\alpha\text{-Fe}$ (mottled) grains.

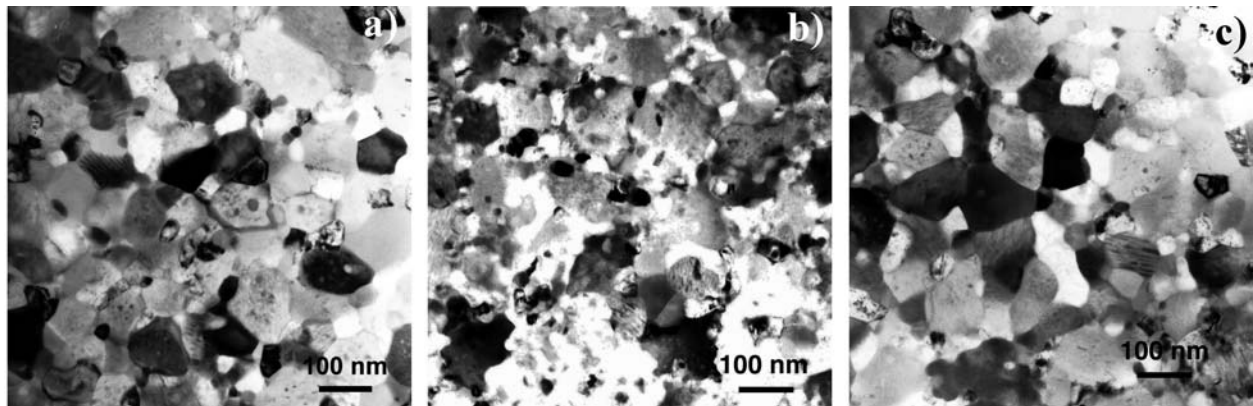


Figure 6 Transmission electron micrographs of the (a) 300°, (b) 400°, and (c) 500°C 2-step anneal samples revealing the formation of a microstructure similar to that seen in the as-spun 1-step anneal with the presence of a second $\alpha\text{-Fe}$ morphology (nanoparticles).

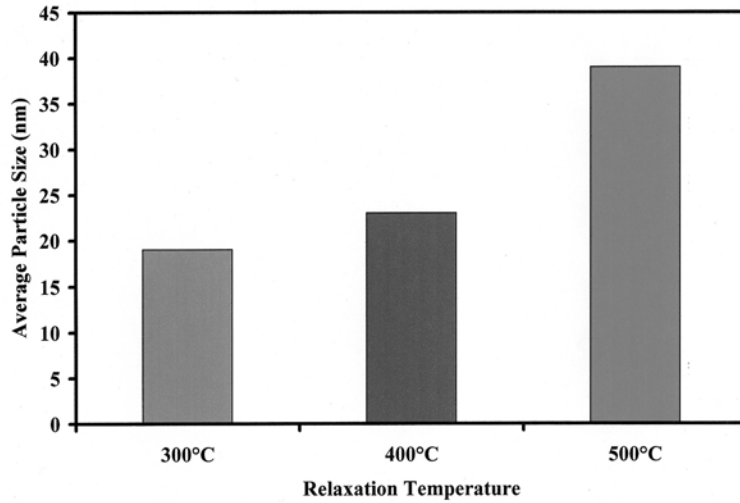


Figure 7 Development of α -Fe nanoparticles as a function of the low-temperature annealing temperature used in the 2-step anneals.

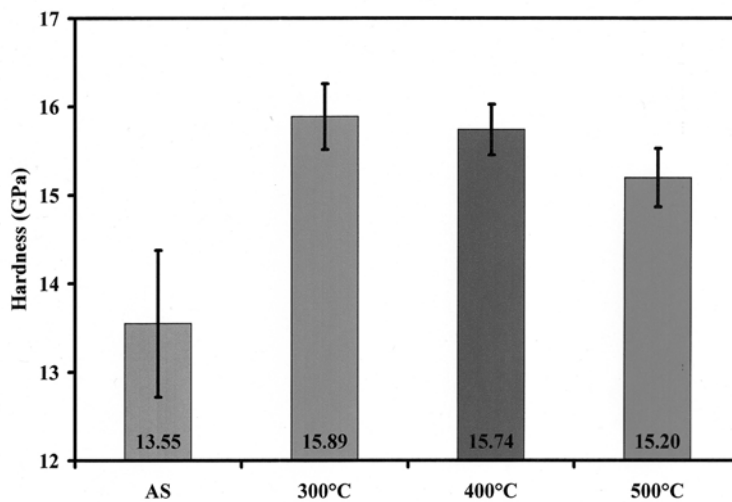


Figure 8 Evolution of Vickers microhardness as a function of the low-temperature annealing temperature used in the 2-step anneal samples. The as-spun 1-step anneal sample (AS) provides a benchmark for examination of the hardness of the material.

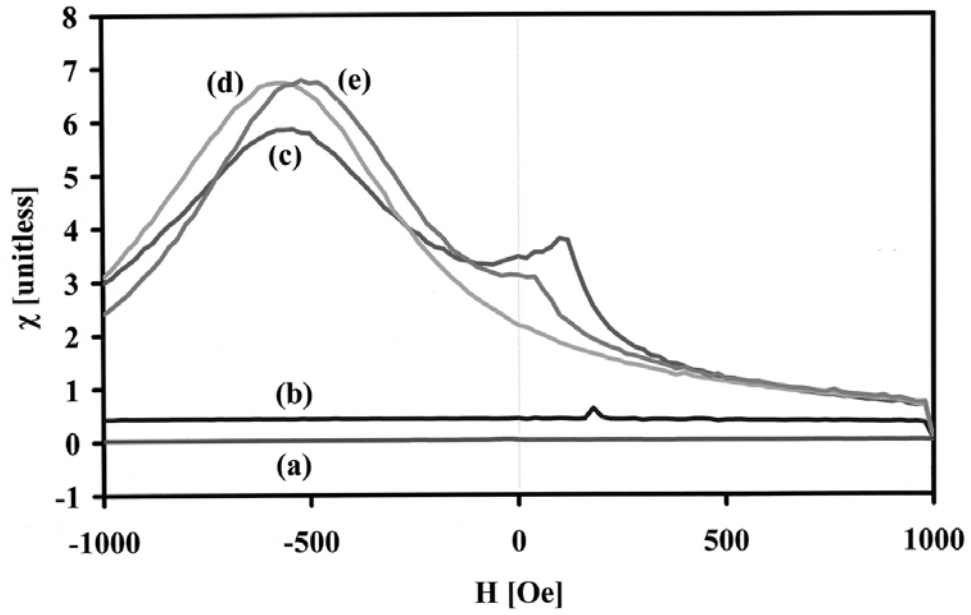


Figure 9 Magnetic susceptibility curves for the (a) 300°C 1-step anneal, (b) 400°C 1-step anneal, (c) 500°C 1-step anneal, (d) as-spun 1-step, and (e) 300°C 2-step anneal samples. The ferromagnetic phases reversing in the first quadrant is attributed to the formation of α -Fe nanoparticles (see text).

References

- ¹ C.K. Majumdar, Phys. Rev. 160 no. 2 (10 August 1967), 430-437.
- ² T. Komatsu, S. Sato, K. Matusita, J. Non-Crys. Solids 91 (1987), 52-62.
- ³ H. Friedrichs and H. Neuhäuser, J. Phys.: Condens. Matter 1 (1989), 8305-8318.
- ⁴ P. Vojtaník, R. Varga, J. Kravčák, A. Lovas, Mater. Sci. and Engg. A226-228 (1997), 736-739.
- ⁵ M. Calvo-Dahlborg, Mater. Sci. and Engg. A226-228 (1997), 833-845.
- ⁶ C. Nagel, K. Rätzke, E. Schmidtke, F. Faupel, W. Ulfert, Phys. Rev. B 60 no. 13 (1 October 1999), 9212-9215.
- ⁷ M.R.J. Gibbs and H.R. Sinning, J. Mater. Sci. 20 (1985), 2517-2525.
- ⁸ V.A. Khonik, J. Non-Crys. Solids 296 (2001), 147-157.
- ⁹ V.I. Belyavsky, K. Csach, V.A. Khonik, V.A. Mikhailov, V. Ocelik, J. Non-Crys. Solids 241 (1998) 105-112.
- ¹⁰ C.K. Majumdar, Phys. Rev. 160 no. 2 (10 August 1967), 430-437.
- ¹¹ M.R.J. Gibbs, J.E. Evetts, J.A. Leake, J. Mater. Sci. 18 (1983), 278-288.
- ¹² J.-P. Bouchard, L. Cugliandolo, J. Kurchan, M. Mézard, Physica A 226 (1996), 243-273.
- ¹³ K. Csach, Y. A. Filippov, V.A. Khonik, V.A. Kulbaka, V. Ocelik, Phil. Mag. A 81 no. 8 (2001), 1901-1915.
- ¹⁴ W. Frank, A. Hörner, P. Scharwaechter, H. Kronmüller, Mater. Sci. and Engg. A179/A180 (1994), 36-40.
- ¹⁵ W. Chambron, F. Lancon, A. Chamberod, J. Non-Crys. Solids 61-62 pt. 2 (January 1984), 895-900.
- ¹⁶ W. Chambron, F. Lancon, A. Chamberod, J. Phys. Lett. 43 no. 2 (15 January 1982), L55-8.
- ¹⁷ M. Calvo, A. Menand, F. Osterstock, J.L. Chermant, MRS Conf.: Rapidly Solidified Alloys and Their Mechanical and Magnetic Properties, 2-4 Dec. 1985, Boston, MA, USA, p. 127-130.
- ¹⁸ M.R.J. Gibbs, J.E. Evetts, J.A. Leake, J. Mater. Sci. 18 (1983), 278-288.
- ¹⁹ E. Woldt, J. Mater. Sci. 23 (1988), 4383-4391.
- ²⁰ G. Cliff, F.W. Lorimer, J. Microsc 103 (1975), 203.
- ²¹ D.J. Branagan and Y. Tang, Composites: Part A 33 (2002), 855-859.
- ²² W. Frank, A. Hörner, P. Scharwaechter, H. Kronmüller, Mater. Sci. and Engg. A179/A180 (1994), 36-40.
- ²³ B.E. Meacham, D.J. Branagan, J.E. Shield, Understanding the Link Between Magnetic Phases and Their Microstructural Scale with Hysteresis Phenomena in Nanoscale Magnets”, J. Magn. Mater., in press..
- ²⁴ W. Frank, A. Hörner, P. Scharwaechter, H. Kronmüller, Mater. Sci. and Engg. A179/A180 (1994), 36-40.
- ²⁵ O.P. Bobrov, V.A. Khonik, V.S. Zhelezny, J. Non-Crys. Solids 223 (1998), 241-249.
- ²⁶ J.D. Verhoeven, *Fundamentals of Physical Metallurgy*, John Wiley & Sons, New York (1975) Chapter 10.
- ²⁷ D.J. Branagan, Y.L. Tang, A.V. Sergueeva, and A.K. Mukherjee, “Low Temperature Superplasticity in a Nanocomposite Iron Alloy Derived From a Metallic Glass”, Nanotechnology, Submitted.